JOURNAL OF SOLID STATE CHEMISTRY 62, 220–230 (1986)

The Magnetic Properties of $FeTa_2O_6$. Magnetic Structure and Low-Dimensional Behavior

S. M. EICHER,* J. E. GREEDAN, AND K. J. LUSHINGTON†

Institute for Materials Research and Department of Chemistry, McMaster University, Hamilton, Ontario L8S 4M1, Canada

Received June 28, 1985; in revised form September 9, 1985

$FeTa_2O_6$ was investigated by X-ray and neutron diffraction, magnetic susceptibility, heat capacity, and Mössbauer effect techniques. The tri-rutile structure was confirmed, space group $P4_2/mnm$. a = 4.749(2) Å, c = 9.192(4) Å and the extent of chemical order between Fe^{2+} and Ta^{5+} was found to be at least 97%. Positional parameters agree well with previous work. A maximum in the magnetic susceptibility versus temperature data occurs at 15(1) K, also in agreement with previous work. Specific heat and neutron diffraction data show that the true Néel temperature for 3-d order is 8.5 K. To explain the high-temperature susceptibility a 2-d Ising model is proposed. A unique solution for the 3-d magnetic structure is found by combining neutron diffraction and Mössbauer effect data.

Introduction

Oxides of composition MTa_2O_6 where M = Mg, V, Fe, Co, and Ni have been known for several years (*1–3*). These compounds crystallize in the trirutile structure due to chemical order between the M^{2+} and Ta^{5+} ions. The space group is $P4_2/mnm$ (No. 136) with M^{2+} ions in positions $2a$ $(000,\frac{111}{222})$ and Ta^{5+} ions in $4e$ $(00 \pm z, \frac{111}{222} \pm z)$. A sketch of the unit cell is shown in Fig. 1. Note that the sublattice formed by the M^{2+} ions has the same symmetry as the Ni^{2+} sublattice in K_2NiF_4, body-centered tetragonal. This observation led us to reinvestigate these materials in search of evidence of low-dimensional magnetic behavior.

Of this series, $FeTa_2O_6$ has been the most widely studied. Polycrystalline magnetic susceptibility data show a maximum at about 13 to 14 K which has been interpreted as the Néel temperature for 3-d ordering (*2, 4*). The crystal and magnetic structures have been reported from powder neutron diffraction data (*5*). In fact, the neutron data are consistent with two possible magnetic structures as will be discussed later. A third magnetic structure has been proposed for $FeTa_2O_6$ from Mössbauer effect data (*4*).

In the following, the results of magnetic susceptibility, neutron diffraction, heat capacity and Mössbauer measurements on $FeTa_2O_6$ are reported. The data give evidence of important low-dimensional magnetic correlations in this material and permit a unique assignment of the magnetic structure. Data for other members of the series will be reported later.

* Present address: Bell Northern Research, P.O. Box 3511, Ottawa K1Y 4H7, Canada.

† Present address: Eastman Kodak Research Laboratories, Bldg. 81, Rochester, N.Y. 14650.

0022-4596/86 $3.00

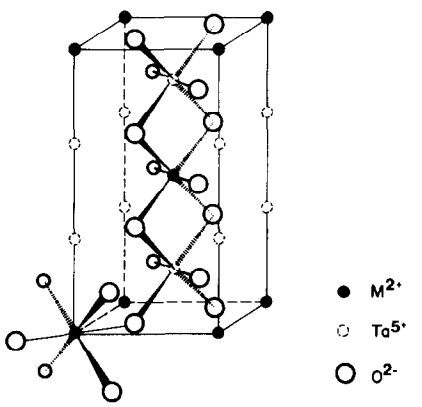

FIG. 1. The trirutile unit cell for MTa_2O_6. The M^{2+} and Ta^{5+} ions are ordered crystallographically. The c axis is tripled with respect to that of a normal rutile unit cell.

Experimental

Preparation. $FeTa_2O_6$ was prepared following Takano and Takada (*4*) from reagent grade Fe_2O_3 (Fisher Chemicals) and Ta_2O_5 (BDH) by solid state reaction in a platinum boat under a reducing buffer gas (CO/CO_2 = 1) at 1100°C. The reaction was normally complete after two 24-hr firings with an intermediate regrinding.

For the Mössbauer measurements about 100 mg of $FeTa_2O_6$ were prepared in the same manner using 100% ^{57}Fe enriched Fe_2O_3 obtained from Oak Ridge National Laboratory.

X-ray powder diffraction. Powder data were obtained for the range $10° < 2\theta < 90°$ with a Philips diffractometer using $CuK\alpha_1$ radiation. Optical grade KCl was added as an internal standard. Unit cell constants were determined from 19 indexed reflections by least-squares refinement.

Powder neutron diffraction. Data were obtained at the McMaster Nuclear Reactor with λ = 1.40 Å. The detector was a single tube linear position sensitive detector which has been described previously (*6*). For room-temperature experiments the samples were held in thin-walled cylindrical vanadium cans of 8 mm diameter. For low temperatures helium-filled aluminum cans of the same diameter, sealed by an indium gasket, were used along with an Oxford Associates cryostat for measurements at 4.2 K and a CTI closed-cycle refrigerator for temperatures above 6.5 K.

Magnetic susceptibility. A Princeton Applied Research vibrating sample magnetometer was employed in fields up to 1.5 T in the temperature range 4.2 to 300 K with an Andonian Associates cryostat. The magnetometer was calibrated with a small nickel sphere.

Mössbauer spectroscopy. Samples of approximately 20 mg (room temperature) and 40 mg (4.2 K) of 100% ^{57}Fe enriched $FeTa_2O_6$ were intimately mixed with Apiezon grease and placed in a 20-mm-o.d. copper holder. For the low-temperature experiments the sample holder was mounted inside a Janis Research cryostat. Temperature was monitored with a calibrated Allen-Bradley carbon resistor. The Elscint transducer and data acquisition system have been previously described (*7*).

Heat capacity. The data were obtained with a calorimeter operating in a continuous heating mode. Samples were pressed pellets weighing about 15 g with a small amount of grease to improve thermal contact to the copper sample tray. A mechanical heat switch was used for initial cooling to liquid helium temperatures to avoid the problem of exchange gas adsorption on the pressed powder samples. The sample tray temperature was monitored by a calibrated germanium resistance thermometer (Lake Shore Cryotronics Inc.).

Data collection was controlled by an online computer which monitored both the temperature and power input to the sample tray. Typical heating rates were 2 to 4 K/hr. Problems with the adiabatic shield made the determination of absolute heat capacities impossible, but transition temperatures and

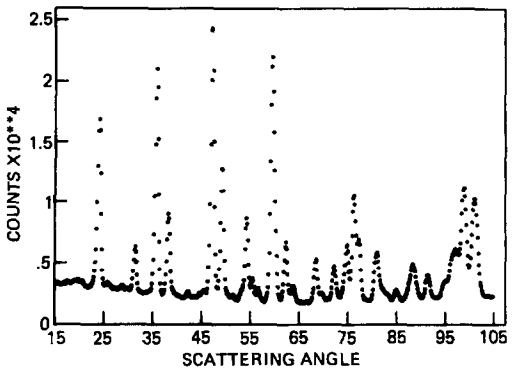

FIG. 2. Neutron powder diffraction data for Fe Ta_2O_6.

the overall morphological details of the data were determined reliably and reproducibly.

Results and Discussion

Crystal Data and Crystal Structure

Since single crystals of $FeTa_2O_6$ are not available all diffraction experiments were performed on powder samples. In particular, the crystal structure was refined from neutron powder diffraction data as shown in Fig. 2. The refinement was based on integrated intensities obtained using the methods described in (*8*). Our results are shown in Table 1 and are compared with those of Weitzel and Klein (*5*).

It is clear that agreement is generally good between the two studies. Our lattice parameters are somewhat larger than those of Weitzel and Klein and of von Heidenstam (*3*), $a = 4.7451(4)$ and $c = 9.179(1)$, but are not significantly different in the limit of three standard deviations.

As mentioned in the introduction, chemical ordering between the Fe^{2+} and Ta^{5+} species gives rise to the trirutile rather than the simple rutile structure. It is clear that the magnetic properties, particularly the existence of low-dimensional correlations, will depend profoundly on the degree of chemical order existing in any given sample. This has recently been shown by Pourroy *et al.* (*9*) for the related trirutile V_2WO_6. In principle, information on chemical order should be available from the neutron diffraction data from the intensities of the trirutile superlattice reflections of the type *hkl* where $l/3 \neq$ integer. In practice, the neutron scattering lengths for Fe and Ta are sufficiently similar that the superlattice peaks are very weak. We have thus chosen to determine the chemical order parameter from X-ray powder data. Integrated intensities were measured for the five most intense superlattice reflections—(002), (101), (112), (211), and (204). These same reflections were calculated using the refined parameters of Table 1 for various degrees of chemical order expressed in terms of the fraction of Fe^{2+} on the 2*a* site. Agreement factors, *R*, were then determined and the results shown in Table 2. From this table it appears that the degree of chemical order is 0.97(2).

Mössbauer data support this conclusion. In Fig. 3 is shown the room-temperature

TABLE 1

CRYSTAL STRUCTURE DATA FOR $FeTa_2O_6$

	This work[a]	Weitzel and Klein
a(Å)	4.749(2)	4.7415(2)
c(Å)	9.192(4)	9.1803(5)
B(Fe)(Å^{-1})	0.7(4)	0.5(1)
Z(Ta)	0.333(2)	0.333(1)
B(Ta)(Å^{-1})	0.5(4)	0.8(1)
X(O1)	0.307(5)	0.309(1)
B(O1)(Å^{-1})	0.4(4)	0.4(1)
x(O2)	0.297(3)	0.2949(5)
z(O2)	0.322(1)	0.3232(4)
B(O2)(Å^{-1})	0.7(3)	0.73(7)
Indep. obs.	29	
Param.	9	
R	3.4	
R_w	2.8	

[a] Neutron scattering lengths were taken as O = 0.58, Fe = 0.95, Ta = 0.691 in units of 10^{-12} cm. Source: L. Köster, H. Rauch, M. Herkens, and K. Schöder, "Summary of Neutron Scattering Lengths," K.F.A., Report, Jül-1755, 1981.

TABLE 2

CHEMICAL ORDER IN $FeTa_2O_6$

Fraction Fe^{2+} in 2*a*	*R*[a]
1.00	0.127
0.99	0.097
0.98	0.071
0.97	0.056
0.96	0.076
0.95	0.067
0.94	0.103
0.93	0.140

[a] $R = \Sigma_i|I_i^\circ - I_i^c|/\Sigma I_i^\circ$.

^{57}Fe spectrum for our sample of $FeTa_2O_6$. This symmetric doublet pattern could be well fitted by a model with a single Fe^{2+} site with isomer shift δ = 1.018(2) mm/sec relative to Fe-foil, quadrupole splitting, ΔE_Q = 3.094(4) mm/sec, and linewidth (FWHM) = 0.376(1) mm/sec. A very weak-shoulder near-zero isomer shift could be identified as an Fe^{3+} contamination at the 3% level with δ = 0.2 mm/sec and ΔE_Q = 0.670(3). Thus our sample appears to be chemically ordered near the 97% level from X-ray data and contains only one detectable Fe^{2+} site from the Mössbauer effect. It is not clear whether the small Fe^{3+} impurity occurs in a separate phase or in solid solution.

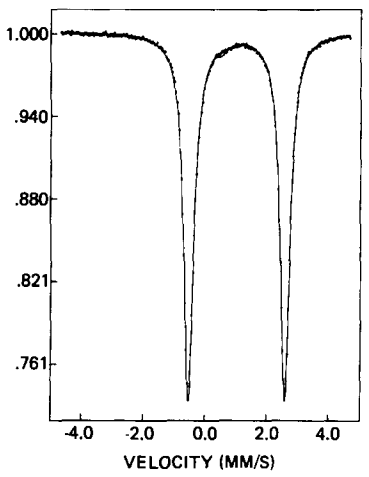

FIG. 3. Mössbauer effect spectrum of $FeTa_2O_6$ at room temperature.

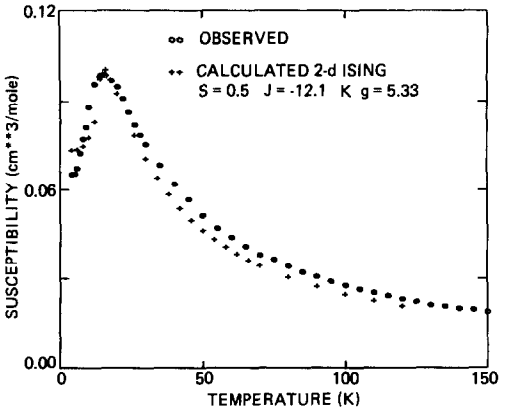

FIG. 4. Magnetic susceptibility of $FeTa_2O_6$ and calculated values for a 2-d Ising model.

Magnetic Properties

Figure 4 shows the low-temperature magnetic susceptibility for polycrystalline $FeTa_2O_6$ and Table 3 gives numerical values of various significant parameters compared with those from previous workers.

Note that the results of three independent studies are in reasonable agreement regarding the susceptibility maximum, χ_{max} and T_{max}, and the Curie-Weiss law constants C and θ.

As mentioned, previous workers have interpreted T_{max} as the critical temperature for 3-d ordering. As the observation of only one thermodynamic quantity is not sufficient to fully characterize a magnetic system, we undertook heat capacity and neutron diffraction measurements.

Figure 5 shows heat capacity data for $FeTa_2O_6$ and isostructural, diamagnetic $MgTa_2O_6$ in the temperature range 5 to 24 K. Due to problems with the mechanical behavior of the $MgTa_2O_6$ sample, its heat capacity obtained by the present method is considered unreliable. The $MgTa_2O_6$ data do provide a semiquantitative indication of the lattice heat capacity which is small rela-

TABLE 3

SUSCEPTIBILITY PARAMETERS FOR $FeTa_2O_6$

	This work	Bernier (2)	Takano and Takada (4)
T_{max} (K)	15(1)	13	14
$\chi_{max} \times 10^{-6} \left(\frac{cm^3}{mole}\right)$	99560(±2%)	95450	94000
$C \left(\frac{cm^3\ K}{mole}\right)$	3.16(1)	3.30	—
θ (K)	−11(1)	−16	−8

tive to $FeTa_2O_6$ and increases monotonically in the temperature interval of interest.

Note the relatively sharp spike at 8.5 K, well below T_{max} of 15 K, and the considerable excess heat capacity for $FeTa_2O_6$ above 8.5 K relative to $MgTa_2O_6$. Such data are typical of systems which exhibit short-range, low-dimensional magnetic correlations at high temperatures and true 3-d ordering at low temperatures. Thus, we assign a critical temperature of 8.5 K for the 3-d magnetic transition in $FeTa_2O_6$ and attribute the susceptibility maximum at 15 K to short-range correlations which appear to be important at temperatures well above 24 K. At this point, it is convenient to discuss the two magnetic regimes separately.

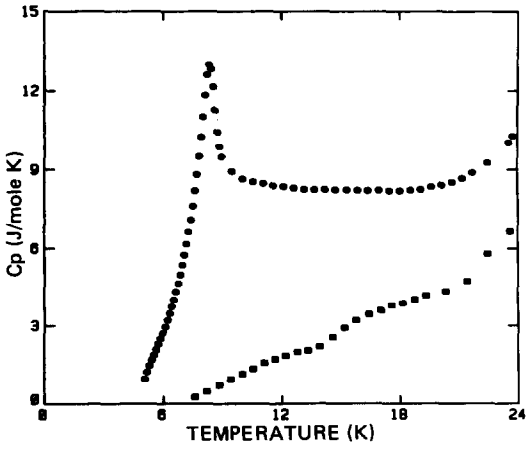

FIG. 5. Heat capacity of $FeTa_2O_6$ (●) and $MgTa_2O_6$ (■).

The 3d-Ordered Regime

We begin with the 3-d-ordered regime as some definite conclusions can be drawn. The existence of true 3-d magnetic order in $FeTa_2O_6$ at 4.2 K was reported by Weitzel and Klein from powder neutron diffraction data (5). We repeated these measurements at 4.2, 77, and 10 K and our results are shown in Fig. 6. The data at 10 and 77 K are essentially identical so only those at 77 K are displayed. The powder pattern at 4.2 K shows new reflections at low angles consistent with 3-d magnetic order. These reflections disappear by 10 K in accord with our assignment of T_c = 8.5 K.

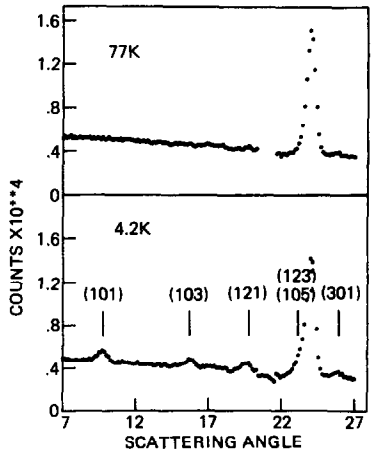

FIG. 6. Neutron diffraction data for $FeTa_2O_6$ at 4.2 and 77 K. Data for 10 K are essentially identical to 77 K and are not shown. Indices are for the magnetic cell $2a$, $2b$, $2c$.

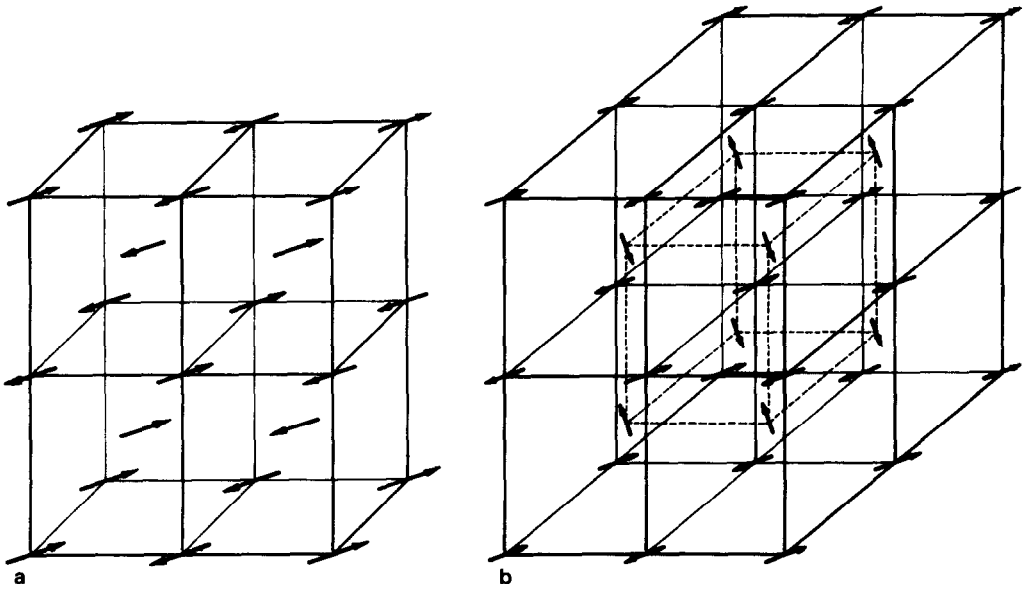

FIG. 7. (a) Model I for the magnetic structure of $FeTa_2O_6$. (b) Model II for the magnetic structure of $FeTa_2O_6$.

The new reflections can be indexed on a magnetic cell which is doubled in the *a* (or *b*) and *c* directions, i.e., either $2a$, b, $2c$ or a, $2b$, $2c$ or $2a$, $2b$, $2c$. These cells are indistinguishable with powder data only. Our results for the magnetic reflections are shown in Table 4 and can be seen to agree well with those of Weitzel and Klein (*5*). According to these workers the data are consistent with two possible magnetic structures for $FeTa_2O_6$ which are shown in Figs. 7a and b.

TABLE 4

COMPARISON OF CALCULATED AND OBSERVED, RELATIVE MAGNETIC INTENSITIES FOR $FeTa_2O_6$

	I_{rel}^{obs}		
hkl[a]	This work	Weitzel *et al.*	I_{rel}^{calc}
101	100	100	100
103	46	46	46.9
121	29	34	33.8
123,105	46	44	45.2
301	8.5	5	7.6
125,303	30	29	22.8
$\mu(Fe^{2+})\mu_B$	3.69(7)	4.01	
R	0.086	0.044	

[a] Indices refer to the magnetic unit cell ($2a$, $2a$, $2c$).

Model I is based on the $2a$, b, $2c$ cell and has moments in the *ab* plane along ⟨110⟩ directions. The moments are antiparallel along ⟨100⟩ and ⟨001⟩ but parallel along ⟨010⟩. Model II is more complex and is based on the $2a$, $2b$, $2c$ cell. It can be thought of as two sublattices of the type of model I displaced by the vector $(\frac{111}{444})$ with the moments of the second sublattice rotated by 90° to the first. That is, the moments of the first sublattice lie parallel or antiparallel to ⟨110⟩ while those of the second are parallel to $\langle\bar{1}10\rangle$. As mentioned these structures are indistinguishable if only powder neutron data are available.

It is possible to distinguish between models I and II using the hyperfine interaction parameters for the ^{57}Fe Mössbauer effect (ME) in $FeTa_2O_6$. The basis for this analysis was established some time ago by Abragam and Boutron (*10*) and Ganiel and Shtrikman (*11*) for rutile structure crystals

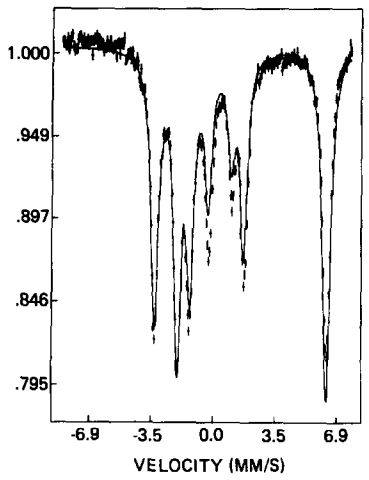

FIG. 8. The Mössbauer effect spectrum of $FeTa_2O_6$ at 4.2 K.

containing Fe^{2+}. In fact, Mössbauer data for $FeTa_2O_6$ were reported by Takano and Takada (*4*) before the neutron diffraction results were available. However, these authors inferred a colinear magnetic structure with Fe^{2+} moments at an angle of 20° to the *c* axis which is clearly inconsistent with the neutron data. Thus, we were led to redetermine and reanalyze the ME hyperfine parameters in $FeTa_2O_6$ at 4.2 K.

The hyperfine Hamiltonian can be written as

$$H_{HF} = H_M + H_Q \qquad (1)$$

where H_M is the effective magnetic field interaction and H_Q is the electric quadrupolar interaction, as given by

$$H_M = -a_0[I_z \cos\theta + (I_x \cos\phi + I_y \sin\phi)\sin\theta]$$

$$H_Q = A_Q[3I_z^2 - I^2 + \eta(I_x^2 - I_y^2)]$$

$$a_0 = g_g\mu_N H_{eff}$$

$$A_Q = \frac{e^2Q_eV_{zz}}{[4I_2(2I_e - 1)]}$$

Here a_0 is the magnetic interaction constant proportional to the effective magnetic field H_{eff}, I is a nuclear spin or spin component, and subscripts g and e refer to ground and excited nuclear states respectively. θ and ϕ are the polar and azimuthal angles, respectively, between the axis of the internal field and the principal axis of the EFG tensor. V_{zz} is the major component of the EFG tensor. $\eta = |V_{xx} - V_{yy}|/V_{zz}$ is the asymmetry parameter and Q is the nuclear quadrupole moment.

The ME spectrum for $FeTa_2O_6$ at 4.2 K is shown in Fig. 8. The spectrum is a complex seven line pattern (an eighth line is very weak) showing clearly the importance of both magnetic and quadrupolar interactions. The parameters obtained from a best fit to the spectrum are shown in Table 5 and compared to those of Takano and Takada (*4*). The fitting of the spectrum was carried out with GMFP5N, a general Mössbauer fitting program due to Ruebenbauer and Birchall (*12*). Transmission integrals were used in the fitting scheme rather than the Lorentzian approximation due to an absorber thickness problem. It can be seen from Fig. 8 that the fit is adequate but that there is a small contribution to the ME absorption which has not been modeled successfully. The most likely source of this discrepancy is the presence of the Fe^{3+} impurity which at low temperatures can contribute over a wide range of velocities. Various attempts to model this contribution were unsuccessful probably because the parameters of this Fe^{3+} site are poorly defined.

TABLE 5

MÖSSBAUER PARAMETERS FOR $FeTa_2O_6$ AT 4.2 K

	This work	Takano and Takada
ΔE_Q (mm/sec)	3.16(3)	3.1
H (KO_e)	251(1)	260
η	0.340(4)	0.2
θ (°)	6(1)	20
ϕ (°)	0	45
FWHM (mm/sec)	0.27(4)	0.43

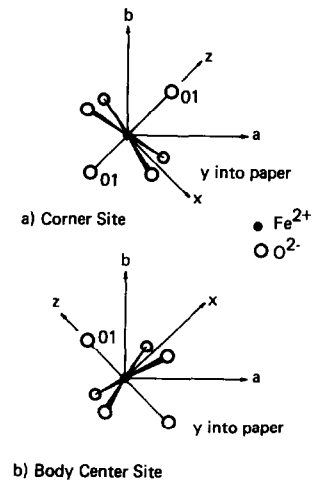

FIG. 9. Molecular symmetry axes and principal axes of the EFG tensor for FeO_6 groups at corner (000) sites and body-center ($\frac{111}{222}$) sites.

Turning to Table 5, there is good agreement between our results and those of Takano and Takada regarding the quadrupole interaction, ΔE_Q, the hyperfine field, H, and the asymmetry parameters, η. The most important discrepancy concerns the angles θ and ϕ. We find θ to be 6(1)°, i.e., the internal magnetic field and the principal axis of the EFG are nearly parallel. Thus the azimuthal angle, ϕ, is essentially undetermined and was set equal to zero in the refinement. Takano and Takada found $\theta = 20°$ and $\phi = 45°$.

The importance of the ME parameters for determining the direction of the magnetic moments in the unit cell will now be described following closely the analysis of Abragam and Boutron (*10*) and Ganiel and Shtrikman (*11*).

The coordinate system in which the orbital part of the Fe^{2+} wave functions are written is shown in Fig. 9. The axes are chosen to be the twofold axes of the distorted FeO_6 octahedron with the z axis along the Fe–O_1 bond and the y axis parallel to the crystallographic c axis. In ideal octahedral symmetry, the orbital wave functions of the excited E_g and ground state T_{2g} multiplets are

$$\begin{matrix} E_g & |xy\rangle \\ & |3z^2 - r^2\rangle \\ & |x^2 - y^2\rangle \\ T_{2g} & |yz\rangle \\ & |xz\rangle. \end{matrix}$$

Under the action of the noncubic field only $|x^2 - y^2\rangle$ and $|3z^2 - r^2\rangle$ can be mixed, the remaining states are already eigen states. The T_{2g} multiplet will then be split into three levels:

$$\psi_1 = a|x^2 - y^2\rangle + b|3z^2 - r^2\rangle \; a \gg b$$
$$\psi_2 = |yz\rangle$$
$$\psi_3 = |xz\rangle.$$

Assuming that the valence electron contribution determines the EFG tensor components it is possible to deduce the ground state wave function from the value of η.

Wavefunctions ψ_2 and ψ_3 give axially symmetric EFGs, i.e., $\eta = 0$, with major axes z and y, respectively. As only ψ_1 is consistent with a nonzero η it is, therefore, the ground state with its major axis along the local z axis. From the magnitude of η the coefficients a and b can be determined using the relationship (*10*)

$$\eta = 2\sqrt{3}ab/(a^2 - b^2)$$

and the normalization condition $a^2 + b^2 = 1$. This leads to

$$\psi_1 = 0.995|x^2 - y^2\rangle + 0.097|3z^2 - r^2\rangle.$$

In the above, spin-orbit coupling is neglected which is justified if the separation between ψ_1, and the excited states is large. The observation of a nearly temperature-independent quadrupole splitting over the range $4.2\ K < T < 300\ K$ seems to support this approach.

Having determined the EFG major axis to the local z axis it is now possible to choose between the two proposed magnetic

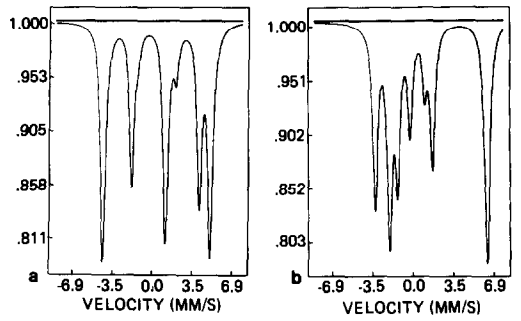

FIG. 10. Simulated ME spectra for $FeTa_2O_6$. (a) $\theta = 0$, $\phi = 0$; (b) $\theta = 90°$, $\phi = 0$.

structures for $FeTa_2O_6$. From Fig. 9, note that the EFG major axis for a corner-site atom (000) is along $\langle 110 \rangle$ while for the body-centered atom $(\frac{111}{222})$ it flips 90° to $\langle \bar{1}10 \rangle$. Returning to Fig. 6 we note that for model I the spin direction does not change on going from (000) to $(\frac{111}{222})$ within the chemical cell while in model II the spins flip by 90° along the EFG axis. Thus for model I the ME spectrum should be a superposition of equal contributions from two sites (i) and (ii) below with different values of θ and ϕ:

(i) $H_m \| z$ $\theta = 0$, ϕ undetermined
(ii) $H_m \perp z$ $\theta = 90°$, $\phi = 0°$.

For model II, only site (i) is expected, which is in fact what was observed. The simulated spectrum for site (ii) above is shown in Fig. 10 and it clearly is very different from that for site (i) and the observed spectrum. One can conclude, therefore, that model II is the true magnetic structure for $FeTa_2O_6$ at 4.2 K.

Short-Range Correlations

The nature of the short-range, noncritical correlations in $FeTa_2O_6$ are more difficult to determine with the same degree of certainty as the 3-d structure. In principle, the magnetic susceptibility in this temperature regime depends on the spin (D) and lattice (d) dimensionalities along with the actual value of the magnetic moment, gS. The unavailability of single crystal data hampers the analysis but some conclusions can be drawn.

First, regarding the lattice dimensionality we have noted already the similarities between the trirutile and K_2NiF_4 structures which would suggest $d = 2$. Interlayer exchange should be weaker than intralayer exchange due to a relatively long, convoluted superexchange pathway and the often-cited symmetry effect (*13*). The intralayer situation is more complex, however, than in K_2NiF_4 as seen from Fig. 10 which shows the (001) projection of four chemical unit cells. Each Fe^{2+} is coupled to its four nearest neighbors (nn) by an intervening oxide ion with a bridging angle of 115° and two unequal bond lengths: one "normal" bond at about 2.1 Å and one very long bond at about 3.5 Å. Next nearest neighbors (nnn) are connected by two different pathways. Along $\langle 110 \rangle$ the exchange involves a linear Fe–O–O–Fe array with Fe–O distances of 2.1 Å and an O–O separation of 2.6 Å. In the $\langle \bar{1}10 \rangle$ direction there are two equivalent M–O–M pathways with long, 3.5 Å, bonds and a 160° bond angle. A priori it is difficult to decide which of these will dominate. Some clue to the relative strengths is provided by the intralayer spin arrangement found in the 3-d ordered state of $FeTa_2O_6$ which is also shown in Fig. 11. From this it is clear that the nnn interactions dominate those of the nn as the moments are antiferromagnetically aligned along $\langle 110 \rangle$ and $\langle \bar{1}10 \rangle$ and it appears that the two different nnn interactions are of similar strength.

For Fe^{2+}, the spin dimensionality can be $D = 3$ (Heisenberg) with $S = 2$, $g \approx 2$, or $D = 1$ (Ising) with effective spin, $S^1 = \frac{1}{2}$ and $4 < g_\parallel < 10$ with $g_\perp \approx 0$ as first shown by Griffith (*14*). Algra *et al.* (*15*) and Engelfriet *et al.* (*16*) have recently found experimental examples of $D = 1$ behavior in Fe^{2+} systems.

All efforts to fit the susceptibility data of

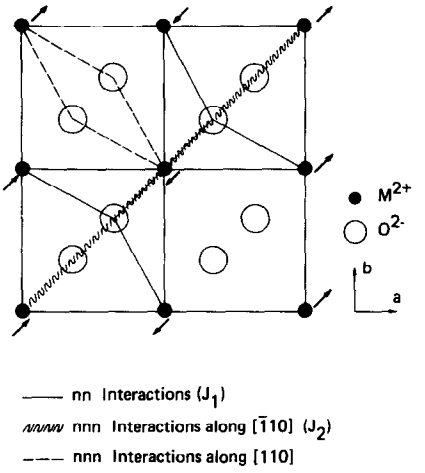

FIG. 11. Superexchange pathways in the *ab* plane for a MTa_2O_6 trirutile. The arrows show the magnetic moments found in the 3-d ordered state for $FeTa_2O_6$.

Fig. 4 using a $d = 2$, $D = 3$ (planar Heisenberg) model with $S = 2$ and a reasonable g factor failed completely. Reasonable agreement in the low-temperature region near the maximum was obtained with a $d = 2$, $D = 1$ model with $S = \frac{1}{2}$, $g = 5.33$, and $J = -12.1$ K as shown in Fig. 4. To model polycrystalline data $\chi_{\parallel}$ and $\chi_{\perp}$ were calculated separately using the series expansion expressions given by Fisher (*17*) and Sykes and Fisher (*18*). It is seen that this model calculates susceptibilities which are too low at high temperatures. A possible explanation for this discrepancy is that the series expansions include the effects of magnetic exchange only and do not account for the van Vleck contributions of the excited levels which become important as the temperature increases.

Summary and Conclusions

A sample of $FeTa_2O_6$ was prepared from Fe_2O_3 and Ta_2O_5 under a reducing buffer gas atmosphere ($CO/CO_2 = 1$). This sample was shown from neutron diffraction, X-ray diffraction, and room-temperature ME data to have the trirutile structure with a degree of order between Fe^{2+} and Ta^{5+} ions of at least 97%. Neutron diffraction and heat capacity data show that $FeTa_2O_6$ undergoes 3-d, antiferromagnetic order below 8.5(1) K, a temperature well below the maximum at 15 K in the susceptibility versus temperature curve. The 3-d magnetic structure at 4.2 K was deduced from two possibilities compatible with powder neutron diffraction data by examination of the hyperfine ME parameters. The susceptibility maximum at 15 K and the excess heat capacity above T_N were assigned to short range order of the $d = 2$, $D = 1$ (planar Ising) type. As this assignment rests largely on the analysis of polycrystalline susceptibility data, single-crystal susceptibility measurements and quantitative heat capacity studies will be required for confirmation.

Acknowledgments

We thank Dr. T. Birchall and Dr. K. Reubenbauer for use of the Mössbauer facilities and assistance with the data collection and interpretation, Dr. C. V. Stager and Mr. G. Hewitson for use of the magnetometer and assistance with data collection, and Mr. J. Couper for assistance with the neutron diffraction experiments.

References

1. J. C. BERNIER AND P. POIX, *Ann. Chim.* **3,** 119 (1968).
2. J. C. BERNIER, *Compt. Rend. C* **273,** 1166 (1971).
3. O. VON HEIDENSTAM, *Arkiv Kemi* **28,** 375 (1968).
4. M. TAKANO AND T. TAKADA, *Mat. Res. Bull.* **5,** 449 (1970).
5. H. WEITZEL AND S. KLEIN, *Acta Crystallogr. Sect. A* **30,** 380 (1974).
6. J. R. D. COPLEY, M. F. COLLINS, K. J. LUSHINGTON, C. V. STAGER, AND P. A. EGELSTAFF, "Neutron Scattering—1981" (J. Faber, Jr., Ed.), pp. 172–174, Am. Inst. Phys. Conf. Proc. No. 189.
7. T. BIRCHALL AND J. P. JOHNSON, *Can. J. Chem.* **57,** 160 (1979).
8. I. J. DAVIDSON AND J. E. GREEDAN, *J. Solid State Chem.* **51,** 104 (1984).

9. G. POURROY, L. PADEL, J. C. BERNIER, G. SCHIFFMACHER, AND M. DRILLON, *Ann. Chim.* **7,** 275 (1982).
10. A. ABRAGAM AND F. BOUTRON, *Compt. Rend.* **252,** 2404 (1961).
11. U. GANIEL AND S. SHTRIKMAN, *Phys. Rev.* **177,** 503 (1969).
12. K. REUBENBAUER AND T. BIRCHALL, *Hyperfine Interactions* **7,** 125 (1979).
13. E. LEGRAND AND R. PLUMIER, *Phys. Status Solidi* **2,** 317 (1962).
14. J. S. GRIFFITH, "The Theory of Transition Metal Ions," p. 355, Cambridge Univ. Press, Cambridge, 1961.
15. H. A. ALGRA, J. BARTOLOME, L. J. DE JONGH, R. L. CARLIN, AND J. REEDIJK, *Physica B* **93,** 114 (1978).
16. D. W. ENGELFRIET, W. L. GROENEVELD, AND G. M. NAP, *Z. Naturforsch.* **35,** 1382 (1980); 852 (1980).
17. M. E. FISHER, *J. Math. Phys.* **4,** 124 (1963).
18. M. F. SYKES AND M. E. FISHER, *Physica* **28,** 919 (1962).